



SCIREA Journal of Hydraulic Engineering

<http://www.scirea.org/journal/Hydraulic>

September 23, 2022

Volume 5, Issue 1, June 2022

<https://doi.org/10.54647/hydraulic57030>

Investigation of water hammer in bending stainless steel pipe under gravity flow

Yujian Ping, Akoto Emmanuel *, Huli Ren

College of Petroleum Engineering, Lanzhou University of Technology, Lanzhou 730050, China

*Corresponding author: akotoe21@yahoo.com

Abstract

A water hammer experimental setup consisting of a 20m long pipe having 8 U-shaped 180° bends is investigated for hydraulic transient. Experimental results are then compared to numerical results simulated by the Method of Characteristics (MOC) and the Wave Characteristic Method (WCM). It is found that one-phase flow one-dimensional models of these numerical schemes are not robust enough to accurately predict the transient phenomenon taking place in such complex pipelines as in the experiment. The two-phase flow one-dimensional models: The Discrete Vapor Cavity Model (DVCM) and Discrete Gas Cavity Model (DGCM), coupled with Vardy & Brown's unsteady friction model obtained more accurate numerical results considering the frequency and magnitude of the peak and minimum pressures of the characteristic curve. Also, these numerical results confirmed the impact of the presence of voids and gases on the wave speed as the reduction of the constant wave speed from 1000m/s in one-phase flow to 700m/s in two-phase accurately simulated the transient phenomenon in the experimental setup.

Keywords: *Hydraulic transient, two-phase flow, cavitation, U-shaped bend, Pressure characteristic curve, DVCM, DGCM, WCM*

1. Introduction

The utilization of pipes, pumps, and valves in the chemical industry and others worldwide can never be overemphasized as they serve as the basic infrastructure for the control of the flow of fluids. And a fluid whether in the gaseous, liquid, multi-phase state, or slurries intrinsically poses unique problems during handling due to its inherent flow properties under different operating conditions. Water hammer is one of these unique engineering problems encountered as a result of control of fluid flow and is not to be taken lightly as it is substantial to the safety of employees and piping installations. A well-known accident case study is that of the Oigawa power station in Japan where water-hammer pressure surges were strong enough to cause the demise of three workers and about half a million dollars in equipment damages [1].

The phenomenon of water hammer was first studied and documented by Joukowsky in 1898 as he was trying to find a way to precisely calculate and measure the pressures generated from this phenomenon [2]. In his studies, he derived the now famous Joukowsky formula used to calculate the maximum and minimum change in pressure surges due to rapid water hammer [3]. For those not well acquainted with this phenomenon, water hammer can be simply defined as a form of fluid transient flow in closed pipes or conduit walls [4]. It describes pressure surges generated by a rapid change of flow velocity in a pipeline [5]. Joukowsky proposed that for fluid flow in closed pipes, the change in maximum pressure is directly proportional to the change in velocity of the fluid flow. Although till now this phenomenon may sound to be simple, in actuality it is very complex due to the nonlinear nature of transient flows. For instance, Michaud [6] in the bid to simplify his work proposed a formula by assuming that the change in velocity is linear. His formula was great but gives poor estimates considering that achieving linear change in velocity is difficult and other valve characteristics were also not factored in. To tackle this problem Wood and Jones introduced two new parameters: a dimensionless valve closure coefficient and dimensionless maximum transient change in pressure parameter [7]. With Joukowsky's formula serving as a boundary limit between rapid and complex water hammer, the magnitude of the transient pressure change can be calculated from the parameters of initial conditions of head drop across the valve gate under the initial conditions of steady flow. By this theory, they developed charts to

individually represent common types of valves and their relationship between these two new dimensionless parameters with respect to the initial steady-state conditions. This was a significant breakthrough even though the effect of frictional losses in transient flow was not considered and the valve gate was characterized by a constant resistance coefficient calculated at a steady flow.

Water hammer mostly occurs in two mechanisms: rapid water hammer and complex water hammer. These two are distinguished by the time it takes for the transient flow-induced propagated wave to be reflected to its source. In the case of a valve-induced water hammer, it becomes rapid in a situation where the time of closing the valve gate is shorter than the return time of the reflected wave. The reverse situation whereby the time of closing the valve gate is greater than the return time of the reflected wave produces the complex water hammer effect [4, 8]. Engineering practice mainly identifies pump-valve operational dynamics, rapid ejection of air out of partially opened valve gate or vent, and collapse of vapor pockets as leading causes of water hammer [2,4]. Hence, there is critical attention paid to the selection and design of pipe profiles, pump-valve instrumentation control, and implementation of surge control devices to ensure piping systems are well protected against this mechanical hazard. A lot of research has been undertaken over the years to better understand the physics of controlling this phenomenon. Marcinkiewicz et al [9] and Pires et al [10] realized in their study that depending on the kind of valve installed, the prolongment of the valve gate closure time can result in a reduction of the maximum pressure [11]. Later on, frictional models like Darcy-Weisbach and Hazen-Williams friction models were derived to account for the effect of internal pipe friction on water hammer [12]. From the Joukowsky formula, it is very clear that the maximum change in pressure is significantly influenced by two physical parameters namely: the speed of the propagated sound wave, and the density of the fluid which represents the nature of fluid compressibility [2]. Assuming that these two parameters are constant during transient flow gives satisfactory results in the calculation of a single-phase water hammer. However, the formation of vapor or void pockets and their collapse presents a case of a two-phase water hammer, and studies have shown that this assumption might not necessarily be valid in such an instance. Benchmark laboratory experiments from Bergant et al [13] and Soares et al [14] attest to this fact. Of the several theories proposed, the Discrete Vapor Cavity Model (DVCM) and Discrete Gas Cavity Model (DGCM) have been found to be more accurate in the calculation of hydraulic transient in two-phase flow [2].

Various numerical schemes coupled with friction and cavitation calculation models have been employed in the computation of water hammer with the Method of Characteristics (MOC) head above the rest. Comprehensive reviews by Mohamed et al [15] and Susovan et al [16] expound on the details of the intricacies related to these numerical approaches. This paper attempts to apply the MOC and the Wave Characteristic Method (WCM) to investigate the phenomenon of the hydraulic transient in a laboratory setup of winding stainless steel pipe under gravity flow. This case study is unique as researchers resort to using straight pipes in experimental studies.

2. Numerical Approach

Mathematical modeling and computer simulation in the investigation of water hammer phenomenon is now considered orthodox as the accuracy and consistency of numerical results have greatly improved over time. Hydraulic transient in any pipe setup can be described by the below one-dimensional partial differential equations (PDE) derived from continuity and momentum equations.

$$\frac{\partial H}{\partial t} + \frac{Q}{A} \frac{\partial H}{\partial x} + \frac{a^2}{gA} \frac{\partial Q}{\partial x} - \frac{Q}{A} \sin(\theta) = 0 \quad (1)$$

$$\frac{\partial Q}{\partial t} + \frac{Q}{A} \frac{\partial Q}{\partial x} + gA \frac{\partial H}{\partial x} + AJ = 0 \quad (2)$$

Where H represents the piezometric head, t is the time, Q the volumetric flow rate, A pipe cross-sectional area, x is the spatial coordinate along the center of the pipe, a is the sound wave speed, g is the acceleration due to gravity, θ is the inclination of the pipe and J representing the friction term.

2.1. Method of Characteristics (MOC)

This method is a grid-based numerical scheme used to solve initial value problems for first-order PDEs. Through this approach, the positive and negative characteristic line equations of the above PDEs are obtained and solved:

$$C^+ : \begin{cases} \frac{dQ}{dt} + \frac{gA}{a} \frac{dH}{dt} + AJ - \frac{gQ}{a} \sin(\theta) = 0 \\ \frac{dx}{dt} = \frac{Q}{A} + a \end{cases} \quad (3)$$

(4)

$$C^- : \begin{cases} \frac{dQ}{dt} - \frac{gA}{a} \frac{dH}{dt} + AJ + \frac{gQ}{a} \sin(\theta) = 0 \\ \frac{dx}{dt} = \frac{Q}{A} - a \end{cases} \quad (5)$$

(6)

By some substitutions, integration along grid coordinates in figure 1, Eq. 3 to 6 can be further simplified to:

$$C^+ : H_p = C_p - BQ_p \quad (7)$$

$$C^- : H_p = C_M + BQ_p \quad (8)$$

Where H_p and Q_p head and volume flow rate at point p respectively, $B = \frac{a}{gA}$, C_p and

C_M derived by Eq. 9 and 10:

$$C_p = H_{i-1} + BQ_{i-1} - JQ_{i-1}|Q_{i-1}| \quad (9)$$

$$C_M = H_{i+1} + BQ_{i+1} - JQ_{i+1}|Q_{i+1}| \quad (10)$$

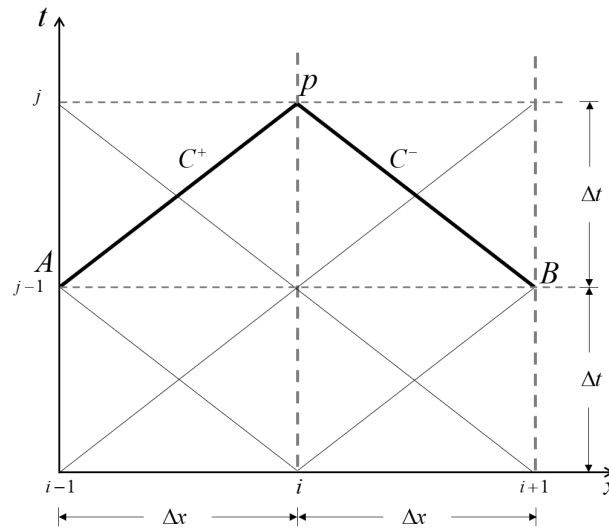


Figure 1. Characteristic lines of MOC having a constant slope

2.1.1. Two Phase Hydraulic Transient Using MOC

Cavitation occurs in a fluid when pressures fall below the vapor pressure and this has significant ramifications on water hammer. To accurately calculate water hammer in such a scenario, it is paramount to consider hydraulic transient in a two-phase flow. The existence of voids and the collapse of vapor pockets affect the wave speed and density of the fluid. This is because the gas-liquid mixture and void fraction directly affect the bulk modulus of the fluid which is a key parameter in the calculation of the sound wave (a') as seen in Eq. 11:

$$a' = \sqrt{1 + \frac{\frac{K_m}{\rho_m}}{1 + \left(\frac{K_m D}{Ee}\right) c_1}} \quad (11)$$

Where D is the nominal diameter of the pipe, E is the Young's modulus of pipe, e is the pipe wall thickness, c_1 is resistance to longitudinal movement factor, K_m and ρ_m are the bulk modulus and density of mixture respectively and are calculated by Eq. 12 and 13:

$$K_m = \frac{K_l}{1 + \alpha \left(\frac{K_l}{P_g} - 1 \right)} \quad (12)$$

$$\rho_m = \alpha \rho_g + (1 - \alpha) \rho_l \quad (13)$$

Where K_l is modulus of liquid, α is the void fraction, P_g is the absolute partial pressure of gas, ρ_m , ρ_g and ρ_l is density of mixture, gas and liquid respectively. By substitution and the assumption that $\rho_m \approx \rho_l$ the wave speed can be calculated with respect to the absolute partial pressure of the gas. This results in a varying wave speed which poses a problem when setting up the equations of MOC on a structured grid. To solve this problem, it is therefore assumed that all the free gas forms single pockets of gas at the nodes and so the wave speed between each node is constant just as in single phase hydraulic transient. This assumption forms the bedrock of DVCM and DGCM. The size of the gas pocket (V_g) is calculated by Eq. 14:

$$\frac{dV_g}{dt} = Q_{out} - Q_{in} \quad (14)$$

Where Q_{out} and Q_{in} are volumetric flow rates out and in of a node respectively. By integrating Eq. 14 from $t - 2\Delta t$ to time t as illustrated in figure 2 results:

$$V_{g,P} = V_{g,P0} + 2\Delta t (\psi (Q_P - Q_{u,P}) + (1-\psi)(Q_{P0} - Q_{u,P0})) \quad (15)$$

Where $V_{g,P}$ is the gas pocket size at the time t , $V_{g,P0}$ is the gas pocket size at time $t - 2\Delta t$, $Q_{u,P}$ and Q_P are the inlet and outlet volumetric flow rates through the node at the time t , $Q_{u,P0}$ and Q_{P0} are the inlet and outlet volumetric flow rates through the node at time $t - 2\Delta t$, and ψ is the weighting factor responsible for controlling the amount of numerical oscillation that occurs in the simulation. $Q_{u,P}$ is calculated by Eq. 16:

$$Q_{u,P} = \frac{C_P - H_P}{B} \quad (16)$$

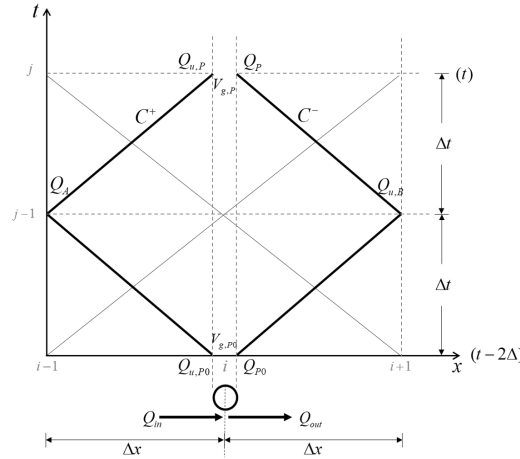


Figure 2. Two-phase flow MOC grid

2.1.2. Discrete Vapor Cavity Model (DVCM)

This model is the simpler of the two assuming that a system in a steady state or having pressures above the vapor pressure, has no vapor or void pockets and hence head is calculated as in a single-phase water hammer. In a transient state and when pressures are below the vapor pressure, the head is treated as a pressure boundary and the difference in volumetric flow rate across the node is converted into vapor or void using Eq. 15 and then stored in the node. This model is however not suitable for simulating high flow scenarios due to the

formation of relatively large vapor cavities. For accurate results, it is recommended to maintain a void fraction below 10% [17].

2.1.3. Discrete Gas Cavity Model (DGCM)

Unlike DVCM, DGCM assumes that there is always some small amount of free gas present in the system and hence calls for mathematical remodeling for the head to be able to account for the effect of the persistent presence of gas vapor. To do this, $V_{g,P}$ is expressed in a new form as shown in Eq. 17 and substituted in Eq. 15 to solve for the head as in Eq. 19:

$$V_{g,P} = \frac{C_3}{H_p - z_p - H_v} \quad (17)$$

$$C_3 = \frac{P_{g,0} \alpha_0 V}{\rho_l g} \quad (18)$$

Where z_p is elevation at point p , H_v is gauge vapor pressure, $P_{g,0}$ is the absolute partial pressure for the initial steady state void fraction α_0 , V is volume of fluid.

$$H_p = \begin{cases} -B_1(1 + \sqrt{1 + B_B}) + z_p + H_v & \text{if } B_1 < 0 \text{ and } B_B > 0.001 \\ -B_1(1 - \sqrt{1 + B_B}) + z_p + H_v & \text{if } B_1 > 0 \text{ and } B_B > 0.001 \\ -2B_1 - \frac{C_4}{2B_1} + z_p + H_v & \text{if } B_1 < 0 \text{ and } B_B < 0.001 \\ \frac{C_4}{2B_1} + z_p + H_v & \text{if } B_1 > 0 \text{ and } B_B < 0.001 \\ \sqrt{C_4} + z_p + H_v & \text{otherwise} \end{cases} \quad (19)$$

Where B_1 , B_B , C_4 are given by Eq. 20:

$$B_1 = -B_2(C_p + C_M) + B_2 B B_v + \frac{z_p + H_v}{2} \quad (20)$$

$$B_2 = \frac{0.5}{2}$$

$$B_v = \frac{\frac{V_{g,P0}}{2\Delta t} + (1-\psi)(Q_{P0} - Q_{u,P0})}{\psi}$$

$$B_B = \frac{C_4}{B_1^2} \quad (20)$$

$$C_4 = \frac{B_2 B C_3}{\psi \Delta t}$$

2.1.4. Friction Model

For friction modeling, a quasi-steady (J_{qs}) and the Vardy & Brown's unsteady (J_{us}) [18] friction models were considered. Where Re is the Reynold's number and ε is dissipation rate of turbulent kinetic energy, J_{qs} can be derived by the following equations:

$$J_{qs} = \frac{fQ|Q|}{2DA^2}$$

$$f = \frac{64}{Re} \quad (\text{for turbulence flow}) \quad (21)$$

$$\frac{1}{\sqrt{f}} = -2.0 \log \left(\frac{\varepsilon/D}{3.7} + \frac{2.51}{Re\sqrt{f}} \right) \quad (\text{for turbulence flow})$$

Vardy & Brown's unsteady friction model (J_{us}) under the assumption that the eddy viscosity at the walls is equal to the laminar viscosity can be derived by:

$$J_{us} = \frac{16\mu}{\rho D^2 A} \left(\frac{\partial Q}{\partial t} * W(\tau) \right)$$

$$\tau = \frac{4\rho t}{\mu D^2}$$

$$W(\tau) = \frac{A^* e^{\tau B^*}}{\sqrt{\tau}} \quad (22)$$

Where $A^* = \frac{1}{2\sqrt{\pi}}$, $B^* = \frac{Re^\kappa}{12.86}$ and $\kappa = \log \left(\frac{15.29}{Re^{0.0567}} \right)$

2.2. Wave Characteristics Method (WCM)

This numerical scheme by assuming a one-dimensional scenario of an elastic fluid of constant mean density tracks the changes surrounding the propagation of the hydraulic transient induced wave. At a point in the system where a disturbance to the flow of the fluid is introduced, stepwise changes in fluid flow rate due to this disturbance over a short period are calculated. After which the incremental pressure pulse as a result of this fluid flow rate change is calculated and propagated at sonic speed through the entire liquid system. By the law of momentum, the characteristics of impedance existing between the pressure and velocity changes along the pipe due to the traveling pulse can be calculated as illustrated in figure 3.

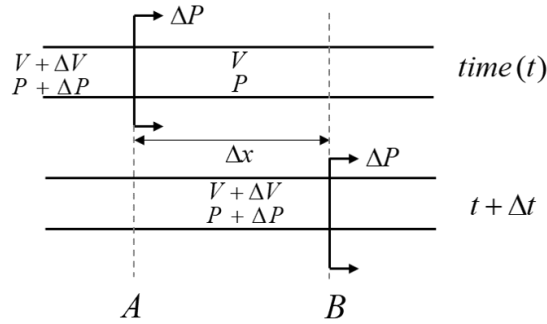


Figure 3. Pressure pulse propagation effect in the pipeline for WCM

$$\begin{aligned}
 (P + \Delta P - P)A &= \rho A \Delta x \frac{\Delta V}{\Delta t} \\
 \Delta P &= \rho \Delta V \frac{\Delta x}{\Delta t} \\
 \Delta P &= \rho a \Delta V \\
 \Delta H &= \frac{a}{g} \Delta V
 \end{aligned} \tag{23}$$

Where P is the pressure of the fluid, A is the cross-sectional area, ρ is the density of the fluid $a \approx \frac{\Delta x}{\Delta t}$ is the wave speed, V is the velocity of the fluid and H is the head of the fluid.

This same principle is expounded to cover all forms of boundary conditions including reflection and transmission of pressure pulse at discontinuities [19]. Friction in WCM is modeled by adding friction orifices. A steady state friction model is selected and simulation is done using the KYPipe Surge 2016 software.

For both numerical analysis, boundary pressure head at the reservoir is set to a constant value and MOC boundary condition for valve is modelled using a dimensionless closure time [20].

3. Experimental Analysis

3.1. Model

The Laboratory apparatus consists of an 800mm x 550mm x 500mm tank (1) at a height of 2050mm connected to a winding stainless steel pipe (2) of a length of 20m and a nominal diameter of 21mm. This pipe has 8 U-shaped 180degree bends and a pneumatic actuated ball valve (3) of a nominal diameter of 25mm installed at the end of the pipe after the last bend. For data acquisition, a pressure sensor (4) mounted just before the ball valve, a Phantom V70 high-speed camera together with related data collection hardware (Model No.: Altai PCI2013) and software suffices (5). Figures 4 and 5 show the water hammer laboratory setup.



Figure 4. Photo of laboratory setup

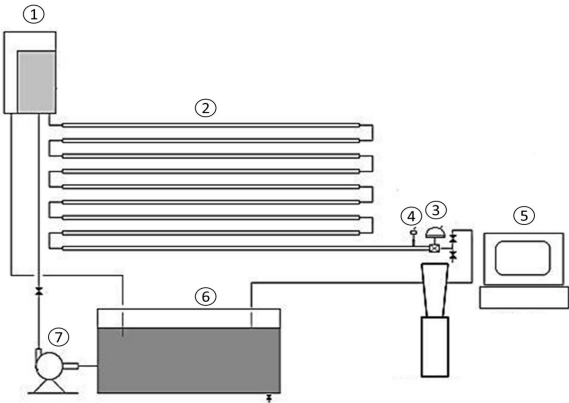


Figure 5. Schematic diagram of laboratory setup

To operate this setup, water of temperature 20°C is pumped (7) from an auxiliary tank (6) into the overhead tank while the ball valve is opened to allow for the initial filling of the pipe.

There is also a flow rate adjustment valve installed on the pipe to regulate flow to a desired velocity. The pump is continuously turned on to sustain a constant water level in the overhead tank. The overhead tank is constructed in such a way as to allow drainage of all excess water being pumped into the tank to maintain a constant water head of 400mm. After ensuring the regulated flow rate is maintained, the ball valve is then closed at set times and speeds. Pressures registered in the pipeline as a result of valve closures at particular flow rates are collected by the sensor and data acquisition device used to interpret results into a readable graph using the software.

The experiment is conducted in two folds: Firstly, the water hammer phenomenon is studied under four different flow velocity regimes (1.443m/s, 1.031m/s, 0.434m/s, 0.116m/s) at the ball valve closure time of 0.35s. And secondly, the phenomenon is investigated for different ball valve closure times (0.35s, 0.47s, 0.68s, 0.93s) at the flow rate of 1.443m/s. The table below highlights the main parameters of this experiment.

Table 1. Main parameters of the experimental setup

No.	Parameters	Specifications
1	Pipe length	20m
2	Pipe thickness	0.002m
3	Pipe nominal diameter	0.021m
4	Pipe material	Stainless steel
5	Pipe roughness	1.3×10^{-6} m
6	Pipe elastic modulus	205GPa
7	Water elastic modulus	2GPa
8	Water temperature	20°C
9	Ball valve diameter	DN25
10	Valve closure times	0.35, 0.47, 0.68, 0.93s
11	Flow velocities	1.443, 1.031, 0.434, 0.116m/s

3.2. Experimental Results

Data from this laboratory experiment is collected in the form of pressure characteristics. The results observed were consistent with that of water hammer literature. This observation can be seen in figures 6 and 7 as the initial spike in pressure increases with respect to the increase in flow rate and reduces when valve closure time is prolonged. It can be seen that for the highest flow velocity of 1.443m/s,

pressure surges from about 6KPa to 900KPa for a valve closure time of 0.35s. And for the longest extended valve closure time of 0.93s at a flow velocity of 1.443m/s, pressure surges from about 6KPa to 95KPa. From the graph, it can also be observed that the pressure peaks keep reducing till the wave finally dampens to a steady state. This is a result of frictional losses in the pipe. The wave frequency also changes with time suggesting changes in the wave speed after every oscillation.

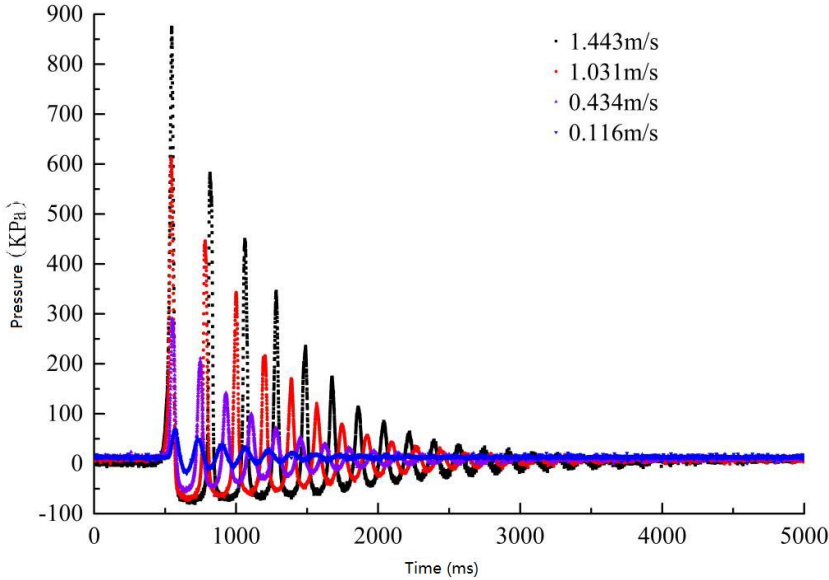


Figure 6. Pressure characteristics for different flow velocities at the valve closure time of 0.35s. (Valve closure signal lags for 0.18s)

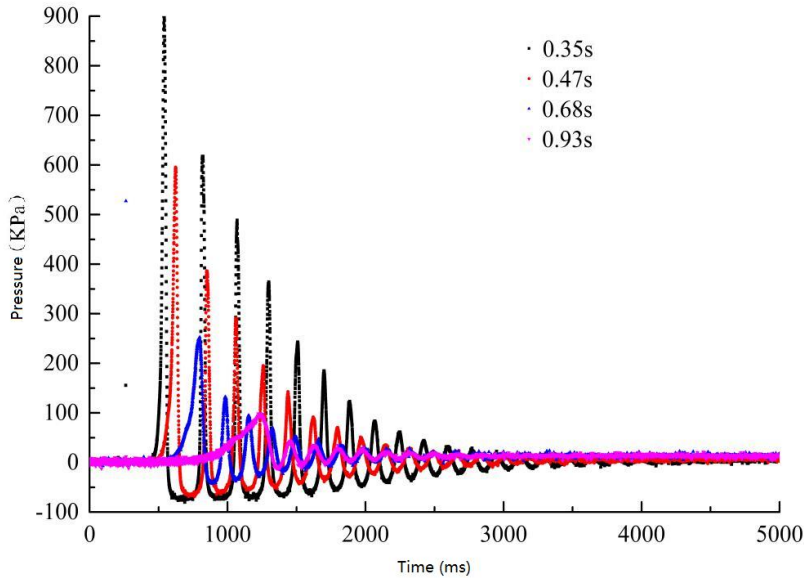


Figure 7. Pressure characteristics for different periods of valve closure times at a flow velocity of 1.443m/s. (Valve closure signal lags for 0.18s)

3.3. Comparison with MOC and WCM

The experimental results of water hammer under flow velocity of 1.443m/s is compared with the MOC and WCM numerical schemes. Firstly, by setting up the numerical schemes to the experimental apparatus parameters and a steady state frictional model, a one-dimensional water hammer without considering cavitation is simulated as shown in figure 8. The result of this simulation shows that these schemes are fairly accurate in predicting the initial pressure spike: 898KPa for the laboratory experiment, 887KPa for MOC, and 942KPa for WCM. However, both numerical schemes after the first spike completely failed to depict the pressure characteristics observed in that of the experiment. To confirm this, the simulation was again run, this time, choosing an unsteady state frictional model. And results yet again did not come close to that of the experiment after the first spike. The presence of the U-shaped bends in the pipe setup has the propensity to introduce bubbles and additional friction which cannot be adequately accounted for in a one-phase flow one-dimensional numerical scheme. The existence of voids and gases in the liquid flow affects the sound wave speed hence affecting the period of wave oscillation. This is not captured in the one-phase numerical scheme and so the pressure characteristics wave oscillates several times for one cycle of the experiment pressure wave.

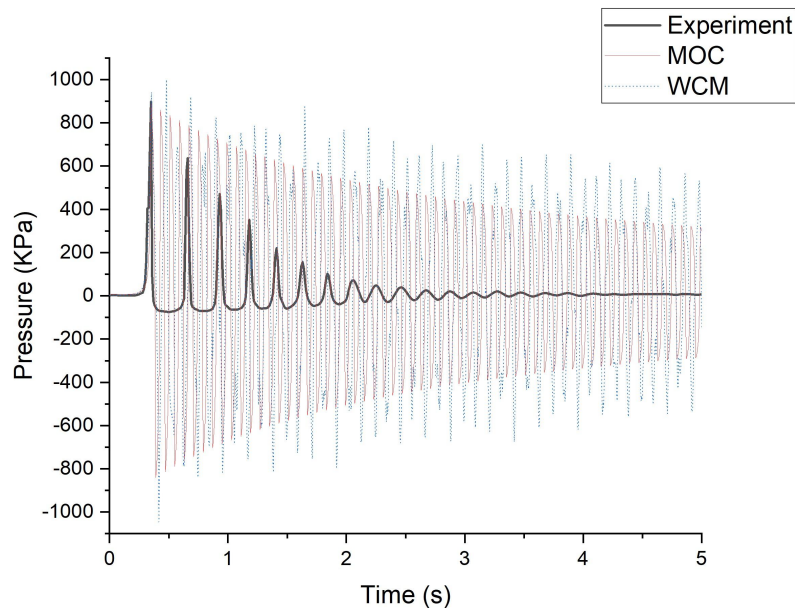


Figure 8. Comparison of pressure characteristics graph of the various schemes without considering cavitation. (Steady friction factor = 0.05, Wave speed = 1000m/s, Flow velocity = 1.443m/s, Valve closure time = 0.35s)

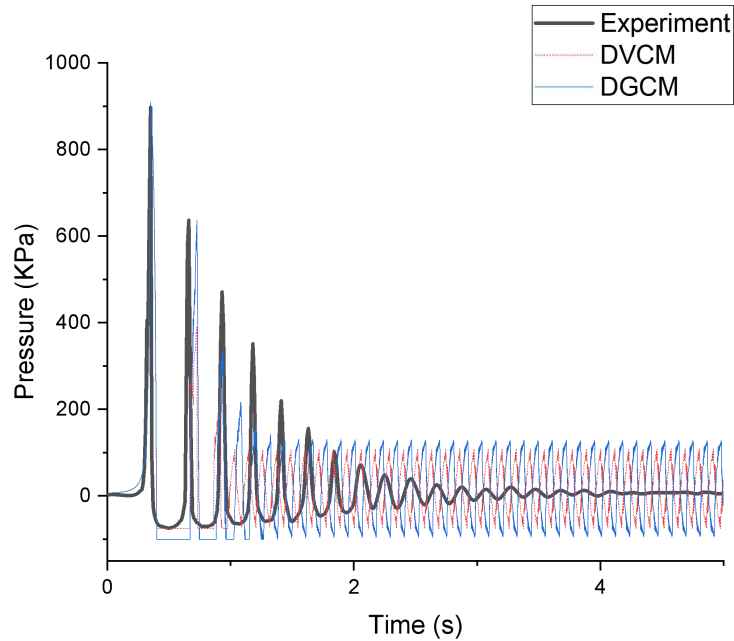


Figure 9. Comparison of pressure characteristics of DVCM and DGCM to experiment. (Unsteady Vardy & Brown friction model, Wave speed = 700m/s, Flow velocity = 1.443m/s, $\psi = 0.75$, Valve closure time = 0.35s)

Now the experimental result is compared to the DVCM and DGCM numerical schemes which take into consideration two-phase flow hydraulic transient. And the result as shown in figure 9 indicates that these two numerical schemes although not completely accurate, better demonstrate the hydraulic transient phenomenon taking place in the laboratory setup. After the third wave cycle, both numerical schemes could not accurately predict the wave frequency and amplitude probably owing to the assumption of constant wave speed between the nodes in DVCM and DGCM. It is also widely known that even the best cavitation models are prone to numerical noise which could lead to some abnormalities in pressures surges [21]. Again, in the simulation setup, the pipe was assumed to be a straight pipe without considering the impact of the U-shaped bends on the energy of the wave and friction losses.

The cavity collapse model for WCM as executed in KYPipe Surge 2016 software is conservative for the purpose of reporting the worst-case scenario as in some situations Joukowski's equation is not accurate in predicting the maximum water hammer pressure [22]. In figure 10, it is seen that due to the conservative nature of the cavitation model, the pressure characteristic curve shows no sign of dampening. In certain instances, very high pressures are recorded indicating the possibility of superposition of waves under this conservative mode.

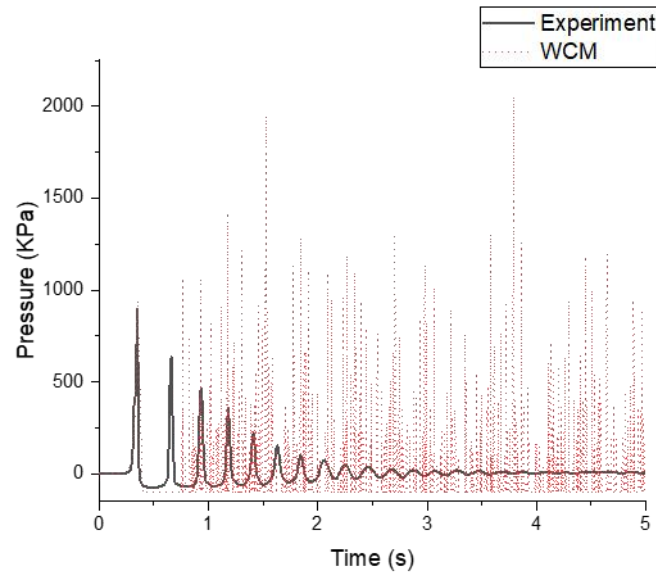


Figure 10. Comparison of pressure characteristics of WCM with cavitation to experiment. (Steady friction model, Wave speed = 1000m/s, Flow velocity = 1.443m/s, Valve closure time = 0.35s)

4. Conclusion

Although the pipe of the experimental apparatus was not straight and had many U-shaped bends, hydraulic transient behavior still adhered to what is generally observed in straight pipelines. Thus, affirming that pressure surges are directly proportional to the increase in the change of fluid flow rate and valve closure times. However, the presence of these U-shape bends tends to harbor gas pockets and voids making the setup a two-phase flow hydraulic transient problem. Results of DVCM and DVGM which are two-phase flow hydraulic numerical schemes confirmed the two-phase flow nature of the experimental setup. The U-shaped bends also probably have a degree of rattle, and thus lose energy causing a reduction in wave speed. DVCM and DVGM numerical schemes are based on the assumption that there is a constant wave speed between nodes and hence do not take into consideration the changes in wave speed due to cavitation and the presence of gas pockets. Nonetheless, the reduction of wave speed from 1000m/s in the single-phase water hammer numerical simulation to 700m/s in the two-phase flow simulation suggests that sound wave loses energy in this regard. Selecting the appropriate wave speed for numerical analysis in this paper was fairly simple due to the availability of laboratory results. Therefore, in the numerical prediction of water hammer in complex pipe geometries, it is paramount that rigorous analysis is carried out with the calculation of wave speed and friction model lest pressure characteristics wave is poorly estimated.

Acknowledgements

The corresponding author would respectfully like to thank the Chinese Government Scholarship Council (CSC) for fully sponsoring his graduate studies.

References

- [1] C. C. Bonin, Water Hammer Damage to Oigawa Power Station, *Journal of Engineering for power*, 82(2),111-116, 1960. <https://doi.org/10.1115/1.3672721>.
- [2] Wylie B. E., Streeter V. L., Suo L., *Fluid Transients in Systems*, Englewood Hills New Jersey, Prentice Hall, 1993.
- [3] Joukowsky, N., “Über den hydraulischen Stoss in Wasserleitungsröhren.” (“On the hydraulic hammer in water supply pipes.”) *Mémoires de l'Académie Impériale des Sciences de St.-Pétersbourg Series 8*, 9(5), 1-71, 1900. (in German).
- [4] Streeter V. L., Wylie B. E., Bedford K. W., *Fluid Mechanics*, WCB McGraw-Hill, New York, 1998.
- [5] Ramos H., de Almeida B. A., Parametric Analysis of Water Hammer Effects in Small Hydro Schemes, *Journal of Hydraulic Engineering*, 128 (7), pp. 689–696, 2002.
- [6] Mitosek M., *Fluid Mechanics in Environmental Engineering*, WNT Warsaw, 2007. (in Polish).
- [7] Wood D. J., Jones S. E., Water-hammer charts for various types of valves, *Journal of Hydraulic Division*, 99(1), 167–178, 1973.
- [8] Thorley A. R. D., *Fluid transients in pipeline system: a guide to the control and suppression of fluid transients in liquids in closed conduits*, ASME Press, New York, 2004.
- [9] Marcinkiewicz J., Adamowski A., Lewandowski M., Flowmaster2™ and program using unsteady wall friction model to calculate water hammer loadings on pipelines, *Nucl. Eng Des*, 238, (8), 2084–2093, 2008. DOI: 10.1016/j.nucengdes.
- [10] Pires L. F. G., Laidea R. C. C., Baretto C. V., *Transient Flow Analysis of Fast Valve Closure in Short Pipelines*, *Proceedings of International Pipeline Conference*, Calgary, Alberta, Canada, 2004.
- [11] Kodura A., An Analysis of the Impact of Valve Closure Time on the Course of Water Hammer, *Archives of Hydro-Engineering and Environmental Mechanics*, Vol. 63, No. 1, pp. 35–45, 2016. DOI: 10.1515/heem-2016-0003.

- [12] Crane Co., Flow of Fluids Through Valves, Fittings, and Pipe, Technical Paper No. 410, Signal Hill CA, 2010.
- [13] Alexandre K. Soares, Nuno Martins, and Dídia I.C. Covas, Investigation of Transient Vaporous Cavitation: Experimental and Numerical Analyses, *Procedia Engineering*, 119:235-242, 2015.
- [14] A. Bergant, U. Karadzic, J. Vitkovsky, I. Vusanovic, and A. R. Simpson, A Discrete Gas-Cavity model that Considers the Friction Effects of Unsteady Pipe Flow, *Journal of Mechanical Engineering*, vol. 51, 2005.
- [15] Mohamed S. G., Ming Z., Duncan A. M., David H. A., A Review of Water Hammer Theory and Practice, *Applied Mechanics Reviews*, vol. 58, 49, 2005. DOI: 10.1115/1.1828050
- [16] Susovan P., Prashanth R. H., Bryan W. K., An Overview of the Numerical Approaches to Water Hammer Modelling: The Ongoing Quest for Practical and Accurate Numerical Approaches, *Water*, 13, 1597, 2021. <https://doi.org/10.3390/w13111597>.
- [17] A. R. Simpsons and A. Bergant., Numerical comparison of pipe-column-separation models, *Journal of Hydraulic Engineering*, vol. 120, 1994.
- [18] A. E. Vardy and J. M. B. Brown, Transient turbulent friction in smooth pipe flows, *Journal of sound and vibration*, vol. 259:1011-1036, 2003.
- [19] Wood D. J., Dorsch R. G., Lightner C. (1965). Wave-Plan Analysis of Unsteady Flow. *Journal of the Hydraulics Division, Proceedings of the American Society of Civil Engineers*, 48, 1965,
- [20] P. G. Provenzano, F. Baroni, and R. J. Aguerre. The Closing Function in the Waterhammer Modeling. *Latin American Applied Research*, 2011.
- [21] Walters T., Marroquin A., Smith F., Understanding Water hammer in Pumping Systems – and Surge Suppression Options, Turbomachinery Laboratory, Texas A&M Engineering Experiment Station, TPS148 Rev 5, 2019.
- [22] Walters, T. W., and Leishear, R. A., 2018, “When the Joukowsky Equation Does Not Predict Maximum Water Hammer Pressures”, ASME PVP Conference, July 15-20, 2018, Prague, Czech Republic, ASME PVP2018-84338, 2018.